JEM Journal of Experimental Medicine

ARTICLE

Inherited IL-18BP deficiency in human fulminant viral hepatitis

Serkan Belkaya[1], Eleftherios Michailidis[2*], Cecilia B. Korol[3,4*], Mohammad Kabbani[2], Aurélie Cobat[3,4], Paul Bastard[1], Yoon Seung Lee[1], Nicholas Hernandez[1], Scott Drutman[1], Ype P. de Jong[2,5], Eric Vivier[6,7,8], Julie Bruneau[4,9], Vivien Béziat[1,3,4], Bertrand Boisson[1,3,4], Lazaro Lorenzo-Diaz[3,4], Soraya Boucherit[3,4], Mylène Sebagh[10], Emmanuel Jacquemin[11,12], Jean-François Emile[13], Laurent Abel[1,3,4], Charles M. Rice[2], Emmanuelle Jouanguy[1,3,4**], and Jean-Laurent Casanova[1,3,4,14,15**]

Fulminant viral hepatitis (FVH) is a devastating and unexplained condition that strikes otherwise healthy individuals during primary infection with common liver-tropic viruses. We report a child who died of FVH upon infection with hepatitis A virus (HAV) at age 11 yr and who was homozygous for a private 40-nucleotide deletion in *IL18BP*, which encodes the IL-18 binding protein (IL-18BP). This mutation is loss-of-function, unlike the variants found in a homozygous state in public databases. We show that human IL-18 and IL-18BP are both secreted mostly by hepatocytes and macrophages in the liver. Moreover, in the absence of IL-18BP, excessive NK cell activation by IL-18 results in uncontrolled killing of human hepatocytes in vitro. Inherited human IL-18BP deficiency thus underlies fulminant HAV hepatitis by unleashing IL-18. These findings provide proof-of-principle that FVH can be caused by single-gene inborn errors that selectively disrupt liver-specific immunity. They also show that human IL-18 is toxic to the liver and that IL-18BP is its antidote.

Introduction

Hepatitis A virus (HAV), hepatitis B virus (HBV), hepatitis C virus (HCV), and hepatitis E virus (HEV) are the most common liver-tropic viruses in humans. HAV and HEV typically cause an acute form of hepatitis, whereas HBV and HCV frequently cause chronic hepatitis, increasing the risk of cirrhosis and hepatocellular carcinoma (Guidotti and Chisari, 2006). HEV may also cause chronic infection (Guidotti and Chisari, 2006; European Association for the Study of the Liver, 2017). In rare cases, primary infections with these viruses, particularly for HAV, HBV, and HEV, can lead to fulminant viral hepatitis (FVH; Liu et al., 2001; European Association for the Study of the Liver, 2017). FVH is defined as severe liver destruction in the absence of preexisting liver disease, leading to encephalopathy within 8 wk of the onset of the first symptoms (Liu et al., 2001; European Association for the Study of the Liver, 2017). It typically strikes children or young adults who are otherwise healthy, with normal immunity to other viruses, bacteria, fungi, and parasites. The actual prevalence and incidence of FVH worldwide are not precisely known, but previous studies have suggested that FVH develops in ≤0.5% of individuals with symptomatic HAV infection (Lemon et al., 2017), with an estimated 1.5 million cases worldwide annually (Lemon et al., 2017). The global incidence of FVH due to HAV has therefore been estimated at ∼1/1,000,000 per year, corresponding to a probable prevalence of 1/100,000. Patients with FVH have a very poor prognosis, with <25% surviving in the absence of liver transplantation. However, survival rates may reach 80% after liver transplantation (Lemon et al., 2017). FVH is typically sporadic, as opposed to epidemic, suggesting that it is not caused by a new more virulent viral strain (Fujiwara et al., 2001; Sasbón et al., 2010; Ajmera et al., 2011).

[1]St. Giles Laboratory of Human Genetics of Infectious Diseases, Rockefeller Branch, The Rockefeller University, New York, NY; [2]Laboratory of Virology and Infectious Disease, The Rockefeller University, New York, NY; [3]Laboratory of Human Genetics of Infectious Diseases, Necker Branch, INSERM U1163, Necker Hospital for Sick Children, Paris, France; [4]Paris Descartes University, Imagine Institute, Paris, France; [5]Division of Gastroenterology and Hepatology, Weill Cornell Medical College, New York, NY; [6]Aix Marseille Université, INSERM, Centre National de la Recherche Scientifique, Centre d'Immunologie de Marseille-Luminy, Marseille, France; [7]Service d'Immunologie, Marseille Immunopole, Hôpital de la Timone, Assistance Publique-Hôpitaux de Marseille, Marseille, France; [8]Innate Pharma Research Laboratories, Innate Pharma, Marseille, France; [9]Department of Pathology, Assistance Publique-Hôpitaux de Paris, Necker Hospital for Sick Children, Paris, France; [10]Department of Pathology, Hepato-biliary Center, Assistance Publique-Hôpitaux de Paris, Paul Brousse Hospital, Villejuif, France; [11]Pediatric Hepatology and Liver Transplantation Unit, National Reference Centre for Rare Pediatric Liver Diseases, Assistance Publique-Hôpitaux de Paris, Bicêtre University Hospital, University of Paris Sud-Saclay, Le Kremlin Bicêtre, France; [12]INSERM U1174, University of Paris Sud-Saclay, Hepatinov, Orsay, France; [13]Department of Pathology, Assistance Publique-Hôpitaux de Paris, Ambroise Paré Hospital, Boulogne-Billancourt, France; [14]Pediatric Immunology-Hematology Unit, Necker Hospital for Sick Children, Paris, France; [15]Howard Hughes Medical Institute, New York, NY.

*E. Michailidis and C.B. Korol contributed equally to this paper; **E. Jouanguy and J.-L. Casanova contributed equally to this paper; Correspondence to Jean-Laurent Casanova: jean-laurent.casanova@rockefeller.edu.

Rare familial cases of FVH have been reported, including two young siblings from a Turkish family, three young brothers from an Iranian family, and two elderly brothers from a Japanese family who developed FVH within weeks of each other following primary HAV infections in their siblings (Durst et al., 2001; Yalniz et al., 2005; Yoshida et al., 2017). In all three families, several relatives of the patients had presented viral hepatitis with a benign course. Inbred strains of mice display differences in susceptibility to mouse hepatitis virus 3 (MHV3; Wege et al., 1982). Upon infection with MHV3, fully susceptible strains (e.g., C57Bl/6J) die from FVH, semisusceptible strains (e.g., C3H/St) develop acute and then chronic hepatitis, and fully resistant strains (e.g., A/J) display no signs of liver disease (MacPhee et al., 1985). These observations suggest that host genetic factors may underlie FVH. The lack of FVH in patients with any of the >350 known primary immunodeficiencies (Picard et al., 2018) suggests that FVH is unlikely to result from inborn errors that broadly disrupt innate and/or adaptive immunity. Instead, previous discoveries that other severe viral diseases striking otherwise healthy individuals, such as epidermodysplasia verruciformis, fulminant EBV disease, herpes simplex encephalitis, severe pulmonary influenza, severe rhinovirus respiratory disease, and severe varicella zoster virus disease, can result from single-gene inborn errors of protective immunity to specific viruses in specific cell types or tissues (Casanova, 2015a,b; Casanova and Abel, 2018) suggest that FVH may result from inborn errors selectively disrupting immunity to hepatitis viruses in the liver. We tested this hypothesis by searching for genetic etiologies of FVH by whole-exome sequencing (WES) in a small cohort of patients.

Results

A private *IL18BP* variation in a patient with FVH

We performed WES on leukocyte genomic DNA (gDNA) from three siblings born to Algerian parents living in France: a girl who died from FVH due to HAV at 11 yr of age with no signs of previous chronic or acute liver disease of any type and her two brothers, who had experienced benign HAV infections (Materials and methods). WES revealed a high rate of homozygosity among the siblings (5.60–6.51%), indicating that this family was consanguineous. We therefore hypothesized that a genetic etiology for FVH in this family would display autosomal recessive (AR) inheritance with complete penetrance. We thus searched for very rare (minor allele frequency [MAF] <0.001) homozygous nonsynonymous variants present in the patient but not in her two siblings (Table S1). Six genes had variants meeting these criteria (Table S2). We prioritized candidate genes for further studies based on (i) the known function of the gene in the liver and/or immunity and (ii) the predicted deleteriousness of the variations. *IL18BP*, encoding the IL-18 binding protein, was the most plausible disease-causing gene, as (i) it encodes a constitutively secreted, naturally circulating neutralizer of the cytokine IL-18 (Aizawa et al., 1999; Novick et al., 1999), the mouse orthologue of which is known to be toxic to the liver (Okamura et al., 1995), and (ii) the patient carried a 40-nt homozygous deletion centered on an intron–exon boundary within this gene. None of the other five variants identified, all of which were missense, had ever been associated with the liver or with immunity (Table S3). Moreover, the *IL18BP* variant (NG_029021.1:g.7854_7893del; NM_173042.2:c.508-19_528del) was not found in any public database (1000 Genomes, dbSNP, Genome Aggregation Database [GnomAD], or Bravo) or in our in-house database of >4,000 exomes, including 65 from unrelated Algerians and ≥1,000 from North Africans (as confirmed by principal component analysis, as in our patient).

Homozygosity for a 40-nt deletion in *IL18BP* segregates with disease

We confirmed by Sanger sequencing that the familial segregation of the mutant *IL18BP* allele was consistent with an AR mode of inheritance with complete penetrance, as both parents and one of the healthy siblings were heterozygous for the mutation, whereas the other sibling did not carry the mutation (Fig. 1, A and B). This mutation, c.508-19_528del, deletes 19 nt from the fourth and last intron and 21 contiguous nt from the fifth and last exon (Fig. 1 B). It is predicted, in silico, to be highly deleterious, with a combined annotation-dependent depletion (CADD) score of 28.2 (Kircher et al., 2014), which is above the mutation significance cutoff (MSC) score of 12.2 for *IL18BP* (Itan et al., 2016; Fig. 1 C). *IL18BP* has a gene damage index (GDI) of 2.05 (Itan et al., 2015), indicating a moderate level of accumulation of nonsynonymous mutations in the general population. Indeed, GnomAD includes only four missense variants (p.V23I, p.R121Q, p.P184L, and p.Q192H) in the homozygous state. Their CADD scores range from 0.001 to 23.3 (Fig. 1 C). Two substitutions, p.R121Q and p.Q192H, are common among Africans, with MAFs of 8.23 and 3.11%, respectively, and the patient was also found to be homozygous for p.R121Q. The other two missense variants, p.V23I and p.P184L, have a global MAF <0.1% (Fig. 1 C). Finally, none of the databases included copy number variations encompassing *IL18BP* in the homozygous state. Collectively, these findings suggested that homozygosity for the private and probably deleterious c.508-19_528del allele in *IL18BP* may be the underlying cause of FVH in this patient.

Mutation c.508-19_528del causes aberrant *IL18BP* mRNA splicing

The canonical *IL18BP* transcript (NM_173042) contains five exons in total, encoding a protein of 194 aa, also annotated as IL-18BPa, with an N-terminal signal peptide (1–30 aa) and an Ig-like domain (31–166 aa) responsible for binding to IL-18 (Fig. 1 D). The c.508-19_528del mutation, which encompasses the last 19 nt of intron 4 and the first 21 nt of exon 5 (encoding aa 170–194), is predicted to impair the splicing of the last exon, thereby affecting the Ig-like domain and the C-terminal part of IL-18BP (Fig. 1 D). We investigated the impact of this deletion on *IL18BP* expression in available material from the patient and other family members. Leukocyte gDNA and liver tissue sections were the only materials available for the deceased patient. In quantitative PCR (qPCR) analyses with different probes detecting various IL-18BPa transcript variants, we found that *IL18BP* mRNA levels in heterozygous EBV-transformed B cells (EBV-B cells) from a sibling and both parents were ∼50% lower than those in homozygous WT cells

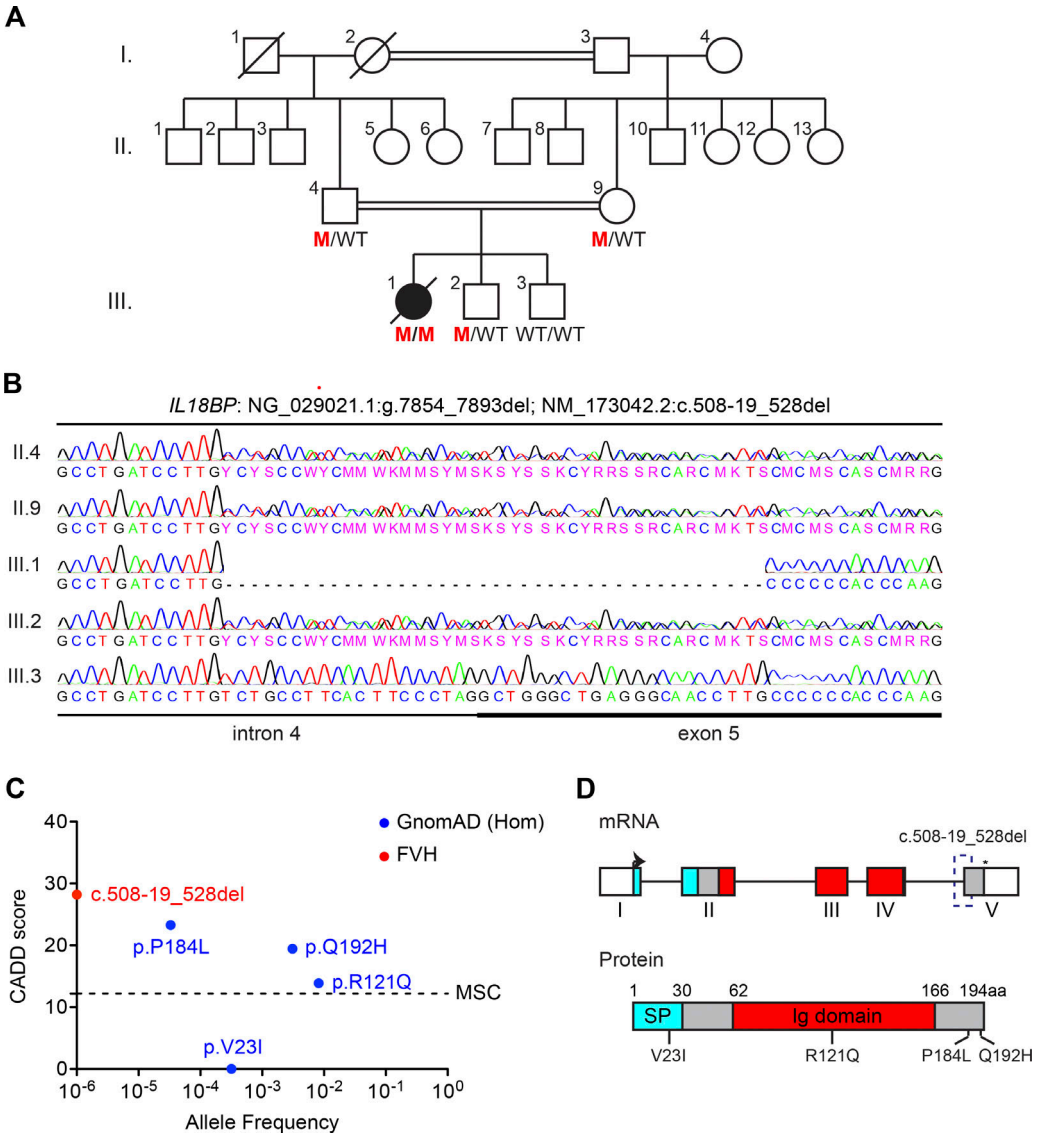

Figure 1. **Homozygous 40-nt deletion in *IL18BP*. (A)** Pedigree of the family affected by FVH due to HAV. The patient is shown in black, whereas healthy individuals are shown in white. Where available, *IL18BP* mutation (NM_173042.2:c.508-19_528del) status is indicated in red. M, mutant. **(B)** Familial segregation of the mutation and its homozygous state in the patient were confirmed by Sanger sequencing. **(C)** Graph showing the predicted CADD scores and global AFs of the mutation found in the patient with FVH (red circle) and missense variants of *IL18BP* (blue circles) for which homozygotes were reported in GnomAD. The CADD-MSC score (90% confidence interval) for *IL18BP* is indicated by a dashed line. **(D)** The upper panel shows the exons (1–5) of the canonical *IL18BP* transcript; the bottom panel shows a diagram for IL-18BP. The signal peptide is highlighted in blue; the Ig domain is shown in red. Start and stop codons are indicated by an arrow and an asterisk, respectively. The c.508-19_528del is shown as a dashed box on the mRNA. The locations of *IL18BP* alleles from GnomAD are also shown on the protein diagram.

from another sibling and healthy controls (Figs. 2 A and S1 A). This suggested that c.508-19_528del was loss-of-expression at the mRNA level. We then amplified the 3′ end of the *IL18BP* cDNA, to determine whether the c.508-19_528del allele generated novel splice variants in the EBV-B cells of the heterozygous sibling (Figs. 2 B and S1 B). We detected three new polyadenylated transcript variants (M1–M3) that also carried the cis p.R121Q mutation (Fig. 2 C). We confirmed these findings through the transient expression of *IL18BP* exons with a 3′ terminal exon-trapping vector (pTAG4) in COS7 cells (Fig. S1, C–E). In particular, M1 and M2 seemed to have no stop codons before the polyadenylation site. However, qPCR on EBV-B cells from WT controls and heterozygous family members showed that all mutant variants were barely detectable and present in much smaller amounts than the WT form (Fig. 2 D). These findings confirmed that c.508-19_528del results in a skipping of the initial sequences of exon 5, without leakiness, and the generation of three novel *IL18BP* transcripts with a shorter terminal exon. Two of these new transcripts have no stop codon, and all three are rapidly degraded. These data suggest that the patient had AR complete IL-18BP deficiency.

Mutation c.508-19_528del disrupts IL-18BP function

We generated cDNA constructs for expression of the three *IL18BP* variants (M1–M3) to assess their impact on IL-18BP

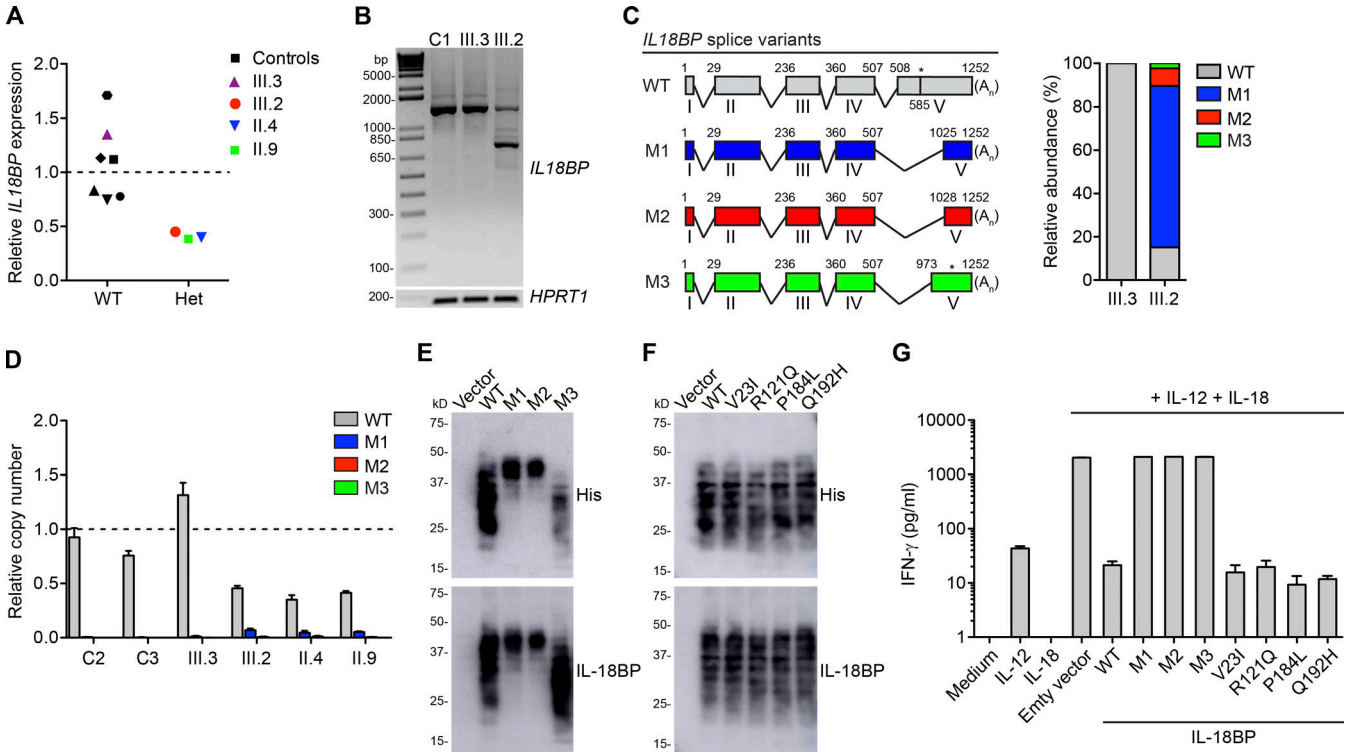

Figure 2. **Impact of the *IL18BP*:c.508-19_528del on gene expression and function. (A)** RT-qPCR showing *IL18BP* levels normalized against endogenous *GAPDH* expression in EBV-B cell lines from six healthy controls (black), the WT sibling (III.3, purple), and heterozygous family members: brother (III.2, red), father (II.4, blue), and mother (II.9, green). Relative *IL18BP* expression was determined by normalization against the mean value for WT cells, set to 1 (indicated by a dashed line). The values shown are the means of two independent experiments performed in duplicate. **(B)** Agarose gel electrophoresis showing aberrant splicing of the *IL18BP* mRNA in 3′ RACE on EBV-B cells from the heterozygous sibling (III.2), relative to a control cell line (C1) and the WT sibling (III.3). *HPRT1* was used as the housekeeping gene control. **(C)** The nested PCR products from B were cloned, and colonies were sequenced. Diagram (left) and percentages (right) of WT (gray) and mutant (M1 in blue, M2 in red, and M3 in green) splice variants of the *IL18BP* transcript are shown. The start codon is located at position 1, and the stop codon is at 585, shown by an asterisk, on the WT transcript. The polyadenylation site is at position 1,252 and indicated by A_n. **(D)** Expression levels of each splice variant (WT in gray, M1 in blue, M2 in red, and M3 in green) were determined and normalized against endogenous *GAPDH* expression levels by RT-qPCR on EBV-B cells from two healthy controls (C2 and C3) and family members. Graph shows the copy numbers of the mutant splice variants relative to the mean copy number for the WT allele in EBV-B cells from C2, C3, and III.3, which was set to 1 (indicated by a dashed line). The values are the means ± SEM of two independent experiments performed in duplicate. **(E and F)** Representative immunoblot images showing levels of the WT and mutant IL-18BP alleles, M1–M3 (E), and four missense alleles from GnomAD (F) in concentrated supernatants from transiently transfected COS7 cells. Immunoblotting was performed with the His tag antibody (top), and the membrane was then stripped and probed with the IL18BP antibody (bottom). **(G)** IL-18BP bioassay: IFN-γ production was measured in NK-92 cells stimulated with recombinant human IL-12 (100 pg/ml), IL-18 (10 ng/ml), and/or concentrated supernatants (100 µg/ml of total protein) of COS7 cells transiently transfected with either empty vector or the constructs expressing indicated IL-18BP variants. Graph is presented on a logarithmic scale with base of 10. The data are the means ± SEM of two independent experiments performed in duplicate using the supernatants shown in E and F and Fig. S1, F and G.

expression and function in vitro. Human IL-18BP migrates at 25–45 kD on SDS-PAGE gels in reducing conditions, due to heterogeneous glycosylation (Kim et al., 2000; Fig. 2 E). We detected abnormal expression of the mutant isoforms (M1–M3) in transiently transfected COS7 cells. M1 and M2 migrated at ∼45 kD, displaying more consistent glycosylation than the WT, whereas M3 had a lower molecular weight but a similar glycosylation pattern to the WT (Figs. 2 E and S1 F). We then analyzed protein production from the four nonsynonymous *IL18BP* alleles found in the homozygous state in GnomAD (the common variants p.R121Q and p.Q192H and the rare variants p.V23I and p.P184L). The pattern of expression of these variants with a C-terminal 6x-His tag in COS7 cells was similar to that of the WT (Figs. 2 F and S1 G). We investigated the functional impact of all variants by an in vitro IL-18BP bioassay in which human IL-18BP inhibits the IL-12/IL-18–induced production of IFN-γ by the natural killer (NK)-92 cell line (Kim et al., 2000; Fig. S1 H). We compared the activity of WT and mutant IL-18BP obtained from the concentrated supernatants of COS7 cells transfected with empty vector, WT, or mutant IL-18BP constructs. All four missense proteins had normal IL-18–inhibiting activity, whereas M1, M2, and M3 did not block IL-18 activity at all (Fig. 2 G). Similar results were obtained for the mutant constructs (M1–M3) generated with or without the common missense allele (p.R121Q) carried by the patient (Fig. S1, I–K). Overall, the c.508-19_528del allele encodes barely detectable M1, M2, and M3 isoforms, all of which lack IL-18–neutralizing function, probably due to their altered protein expression, in terms of pattern and molecular weight. These findings indicate that the patient had AR complete IL-18BP deficiency, whereas individuals from the general population carrying homozygous *IL18BP* variants had normal IL-18BP expression and function. These findings suggest

that AR IL-18BP deficiency is exceedingly rare in the general population and that AR IL-18BP deficiency is probably the cause of FVH in this patient.

Expression patterns of IL-18, IL-18BP, and IL-18R in the liver

Human IL-18 was initially identified from a liver cDNA library as an IFN-γ–inducing factor in NK cells and T cells (Ushio et al., 1996). We analyzed the expression patterns of IL-18, IL-18BP, and the two chains of IL-18R, IL-18R1 and IL-18RAP, in several human cell lines acting as surrogates of liver-resident cells: Hep3B (hepatocytes), HUVECs (endothelial cells), LX-2 (hepatic stellate cells), SV40 fibroblasts, THP1 (monocytes), NKL (NK cells), Jurkat (T cells), and Raji (B cells) cells. We assessed mRNA and protein levels at baseline and following stimulation with various inflammatory cytokines, including IFN-α, IFN-γ, IFN-λ, TNF-α, IL-6, IL-15, IL-18, IL-22, and IL-27 (Figs. S2 and S3). We found that THP1 cells were major producers of IL-18, whereas IL-18 was either present at very low levels or undetectable in other cell types (Fig. S2, A and B). IL-18BP was constitutively expressed only in THP1 and Jurkat cells, and was markedly upregulated by stimulation with IFN-γ, particularly in Hep3B, SV40 fibroblasts, HUVECs, and LX-2 cells (Fig. S2, C and D). Moreover, IFN-α or IL-27 also increased IL-18BP production, albeit to a much lesser extent (Fig. S2, C and D). Of note, we did not detect rare alternative splicing forms of *IL18BP*, namely *IL18BPb*, *IL18BPc*, or *IL18BPd* (Novick et al., 1999; Kim et al., 2000), in HepG2 (hepatocyte) cells, THP1 cells, or primary human hepatocytes, as previously reported to be absent in human peripheral blood mononuclear cells (PBMCs; Veenstra et al., 2002; data not shown). Finally, we found that both chains of IL-18R were expressed principally in NKL cells (Fig. S2, E and F; and Fig. S3). These observations, consistent with previous reports (Lebel-Binay et al., 2000), suggest that IL-18 is mostly produced by macrophages in the liver, and that it induces IFN-γ production, particularly by NK cells, which in turn triggers intrahepatic IL-18BP secretion, mostly from hepatocytes and macrophages. Thus, IL-18BP, which is induced strongly by IFN-γ, can buffer intrahepatic IL-18 activity through negative feedback.

Elevated IL-18 levels in liver tissues of patients with FVH

It has been suggested that the liver lesions observed during the course of acute hepatitis are not directly due to the cytopathic effects of HAV, but instead result from excessive cytotoxic activity of NK, NKT, and $CD8^+$ T lymphocytes (Kim et al., 2011, 2018; Lemon et al., 2017). We thus performed immunohistochemical staining on liver sections from the IL-18BP–deficient patient described in this study, an unrelated patient with FVH due to HAV, and an individual without liver inflammation. Only very small numbers of hepatocytes were detected in the liver tissues of the two FVH patients (Figs. 3 and S4). However, the IL-18BP–deficient patient and the unrelated FVH patient had higher proportions of T cells ($CD3^+$, $CD4^+$, or $CD8^+$), perforin-positive cells (attributed to $CD8^+$ T and NK cells), NK cells ($CD57^+$ or $NKp46^+$), B cells ($CD20^+$), M1 and M2 ($CD68^+$) macrophages, and M2 ($CD163^+$) macrophages than the control individual (Figs. 3 and S4). These observations indicate a massive loss of hepatocytes and inflammatory cell accumulation in the livers of FVH patients. Moreover, the IL-18 staining was abnormally high in the liver tissues of FVH patients. This cytokine was detected in both macrophages and hepatocytes in these patients, whereas it was barely detectable overall and found only in macrophages in healthy liver sections (Figs. 3 and S4). IL-18BP was not detected in liver sections from controls or patients (data not shown; Materials and methods). Collectively, these data suggest that, in baseline conditions, IL-18 is produced mostly by macrophages in the liver, but that hepatocytes also produce IL-18 during viral infection.

Human IL-18 induces NK cell–mediated killing of hepatocytes in vitro

IL-18 increases NK and/or T cell–mediated cytotoxicity by inducing (i) the expression of membrane-bound FasL, an activator of cell death, (ii) the secretion of proapoptotic cytokines, such as TNF-α and TNF-related apoptosis-inducing ligand, and (iii) the secretion of cytolytic enzymes, such as perforin and granzyme (Lebel-Binay et al., 2000; Tsutsui et al., 2000; Kaplanski, 2018). Moreover, IL-18, together with IL-2, enhances the activation and in vitro cytotoxic activity of human peripheral NK cells (Son et al., 2001; Nielsen et al., 2016). IL-2–stimulated human liver NK cells have also been shown to be strongly cytotoxic, even more so than peripheral blood NK cells, to human HepG2 hepatocytes (Ishiyama et al., 2006). We therefore generated an in vitro model to test IL-18/IL-18BP–regulated hepatotoxicity through the coculture of HepG2 and NK-92 cells, which display a phenotype similar to liver-resident NK cells in humans (Le Bouteiller et al., 2002). NK cells activated with IL-18 killed significantly more hepatocytes than unstimulated NK cells at various NK-cell-to-hepatocyte ratios (Fig. S5, A–C). As expected, IL-18BP completely rescued IL-18–induced NK cell–mediated hepatotoxicity (Fig. S5, A–C). We also showed that IL-18, together with IL-2, increased in vitro cytotoxicity of PBMCs from healthy donors against HepG2 cells, and that IL-18BP could prevent the IL-18–induced toxicity (Fig. S5 D). Finally, we infected HepG2 or Huh7.5 hepatocytes with HAV (Fig. S5 E; Materials and methods). We showed that IL-18–activated NK cells killed both infected and uninfected hepatocytes, and that this cytotoxicity was reversed by the addition of IL-18BP (Fig. 4, A and B). Overall, these findings support a model in which the genetically determined absence of IL-18BP in the patient with FVH by HAV leads to uncontrolled IL-18–mediated cytotoxic activity against hepatocytes, involving NK and T cells, the most abundant lymphocytes in the liver, in particular, thereby exacerbating liver destruction (Fig. 4 C).

Discussion

We have established a causal relationship between AR complete IL-18BP deficiency and lethal FVH due to HAV in an 11-yr-old child without preexisting liver disease and with no history of severe infection. Causality is established on both genetic and mechanistic grounds, meeting the criteria for genetic studies in single patients (Casanova et al., 2014). In contrast, it is unclear if the two autoimmune phenotypes of the patient, type I diabetes

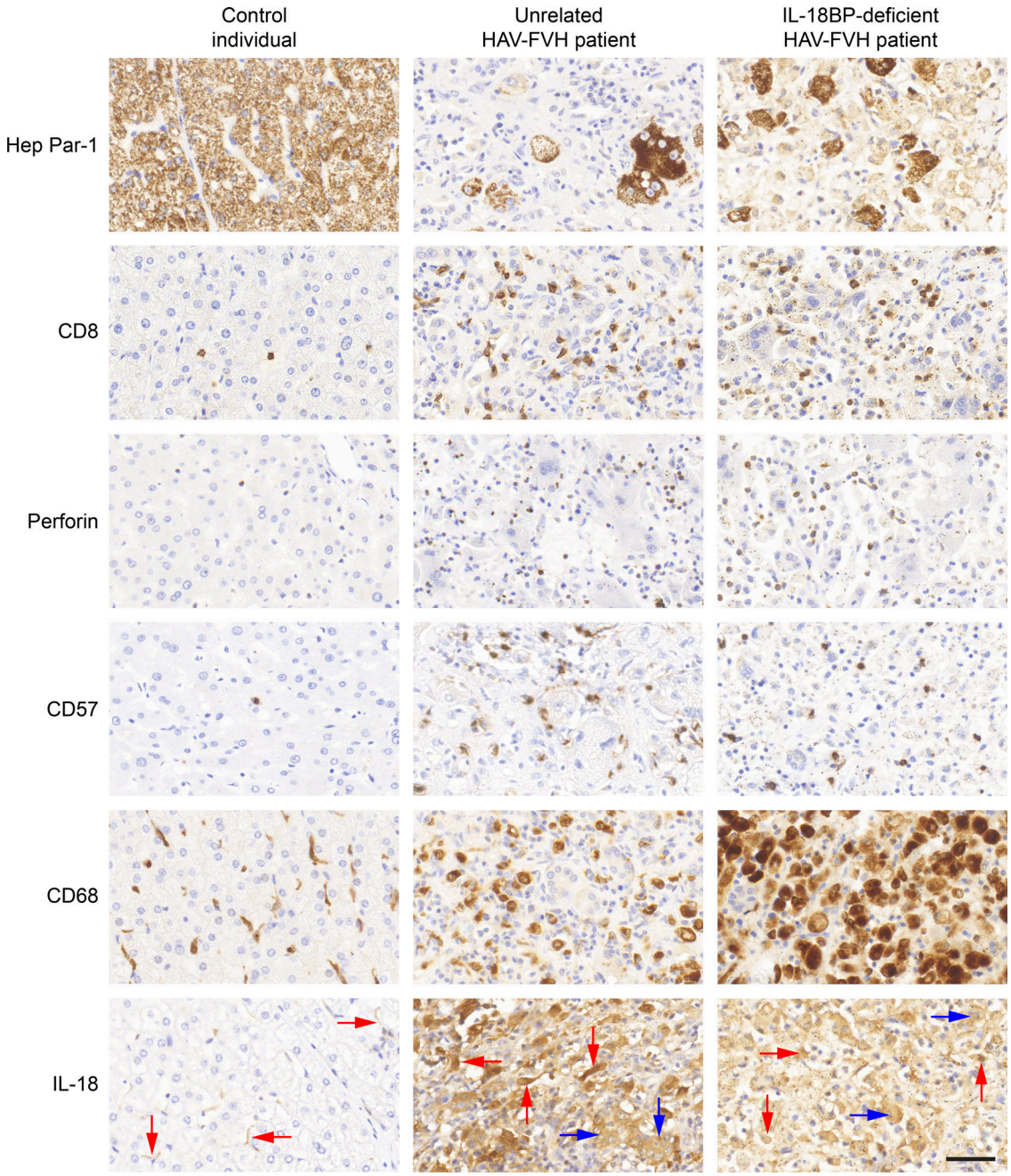

Figure 3. **Liver immunohistochemical profile of the patient.** Liver tissue sections from a control individual, an unrelated patient with FVH due to HAV, and the deceased IL-18BP–deficient FVH patient reported in this study were subjected to immunohistochemical staining with the following markers: Hep Par-1, CD8, perforin, CD57, CD68, and IL-18. Representative zoom-in views of the original images at 400× magnification (Fig. S4) are shown. Hep Par-1 staining of IL-18BP–deficient patient's liver tissue section displayed a background staining of macrophages, with lower intensity than hepatocytes. Some IL-18–positive hepatocytes and macrophages are indicated with blue and red arrows, respectively. Scale bar represents 50 µm.

and Hashimoto's thyroiditis, are also due to IL-18BP deficiency. The child had AR complete IL-18BP deficiency, and there are $\leq 2.5 \times 10^{-8}$ such patients in the general population. IL-18 is a pleiotropic inflammatory cytokine that was initially discovered in mouse liver and has been reported to activate NK cells and T cells in addition to its potent IFN-γ–inducing activity (Kaplanski, 2018). Serum and hepatic concentrations of IL-18 and IFN-γ were high in patients with various forms of fulminant liver failure (Yumoto et al., 2002; Shinoda et al., 2006). In particular, serum IL-18 was found to be dramatically elevated in patients with acute hepatitis due to HAV infection (Kim et al., 2018). Moreover, mouse IL-18 has been shown to induce intrahepatic inflammatory cell recruitment and severe hepatotoxicity in various liver injury models (Tsutsui et al., 2000; Finotto et al., 2004; Kimura et al., 2011), whereas IL-18BP has been shown to protect against IL-18–mediated fulminant hepatitis in mice (Faggioni et al., 2001; Fantuzzi et al., 2003; Shao et al., 2013). Our findings indicate that uncontrolled IL-18 activity in humans is

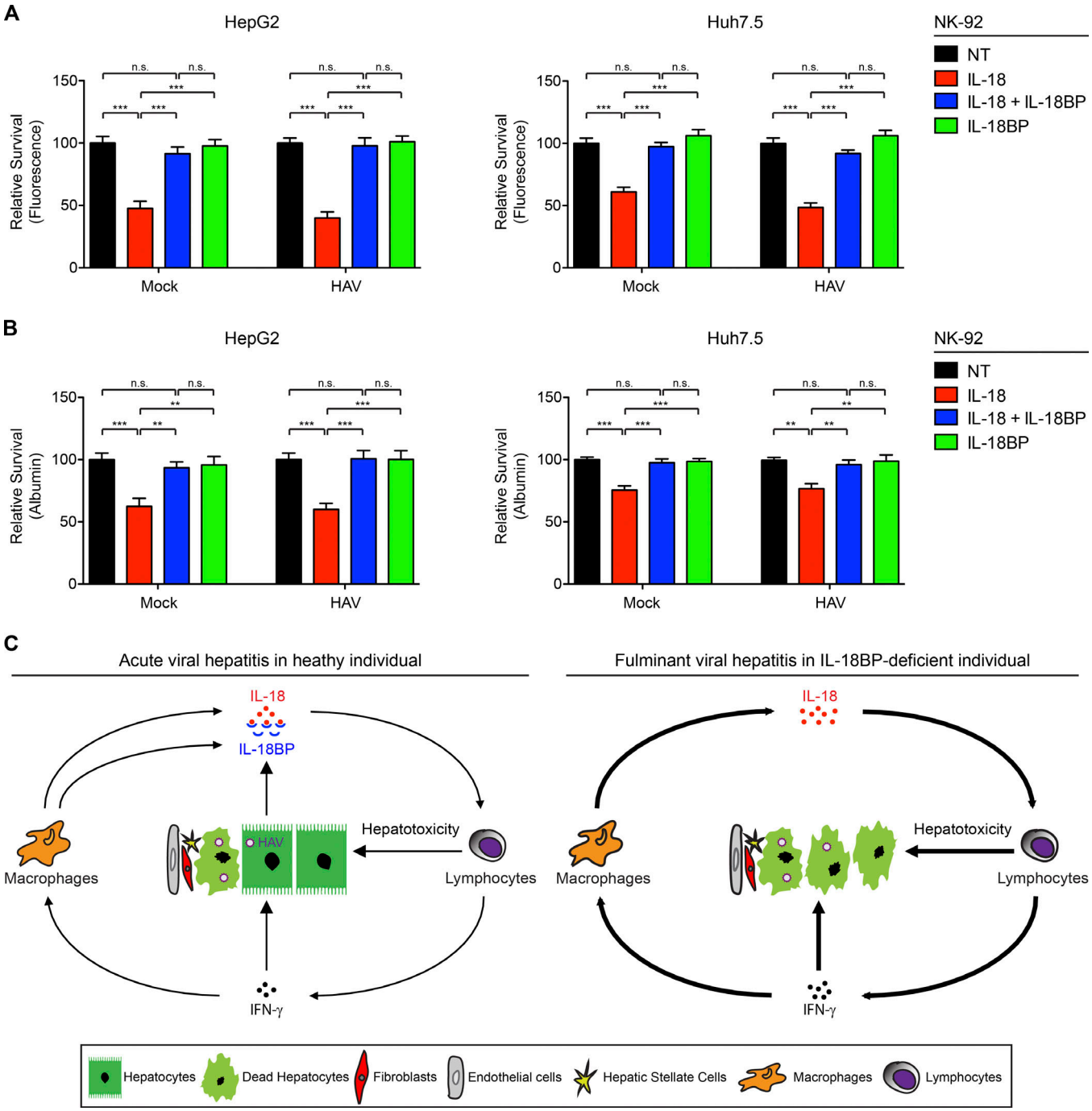

Figure 4. **IL-18/IL-18BP–mediated hepatotoxicity. (A and B)** Coculture of mock- or HAV-infected hepatocytes (HepG2 and Huh7.5 cells) with NK-92 cells pretreated with IL-18, IL-18 + IL-18BP, or IL-18BP. HAV infection efficiencies in HepG2 and Huh7.5 cells were ∼40% and ∼100%, respectively (Fig. S5 E; Materials and methods). The relative survival of calcein-AM–stained HepG2 or Huh7.5 cells was calculated based on the measurement of fluorescence retention within cells (A) and the amount of secreted albumin (B). Relative fluorescence and albumin levels were determined by normalization against the mean value for hepatocytes cocultured with NK92 cells without pretreatment (not treated [NT]), set to 100. A decrease in the fluorescence or in albumin levels indicates an increase in NK cell–induced hepatotoxicity. The data shown are the means ± SEM of three independent experiments performed in quadruplicate (n.s., not significant; **, $P < 0.01$; ***, $P < 0.001$; one-way ANOVA with Bonferroni correction for multiple comparisons). **(C)** A proposed model for IL-18BP deficiency underlying FVH. During the course of acute HAV infection in an otherwise healthy individual (left), IL-18 is secreted by macrophages in the liver. This cytokine activates lymphocytes, such as NK cells, inducing IFN-γ production and cytotoxicity to eliminate HAV-infected cells. IFN-γ also induces IL-18BP secretion by hepatocytes, macrophages, and other nonparenchymal cells (endothelial cells, fibroblasts, and hepatic stellate cells), to buffer IL-18 activity. However, in the absence of IL-18BP (right), excessive IL-18 activity leads to uncontrolled, massive immune-mediated hepatotoxicity and severe liver injury, as in the IL-18BP–deficient individual with FVH.

toxic to the liver, as previously demonstrated in mice, and that human IL-18BP is a potent liver-protective compound, acting as an antidote to IL-18. Recombinant human IL-18BP (Tadekinig Alfa; AB2 Bio) has been approved for clinical use for indications unrelated to liver conditions and proposed as a treatment for preventing acetaminophen hepatotoxicity (Bachmann et al., 2018). We provide proof-of-principle that FVH can be caused by single-gene inborn errors of immunity to HAV in the liver. Our findings also reveal the essential functions of IL-18 and IL-18BP in humans. By inference from previous human genetic study of other isolated infections, which are characterized by genetic heterogeneity but physiological homogeneity (Casanova, 2015a,b; Israel et al., 2017; Tangye et al., 2017; de Jong et al., 2018; Hernandez et al., 2018; Martínez-Barricarte et al., 2018; Zhang et al., 2018), there might be other genetic etiologies of FVH that impair IL-18BP or enhance IL-18 activity. Furthermore, neutralizing endogenous IL-18, particularly with recombinant IL-18BP, might be beneficial to patients with FVH caused by HAV and possibly other viruses.

Materials and methods

Patient recruitment and ethics

Clinical history and biological specimens were obtained from the referring clinicians, with the consent of the patients and family members participating in the study. All the experiments involving human subjects conducted in this study were in accordance with institutional, local, and national ethical guidelines and approved by the French Ethics Committee, the French National Agency for the Safety of Medicines and Health Products, the French Ministry of Research (protocol C09-18), and the Rockefeller University Institutional Review Board (protocol JCA-0700).

Case report

The patient (III.1) was born in France in 2002 to consanguineous Algerian parents. In 2004, she was diagnosed with insulin-dependent diabetes. Tests for anti–islet cell and anti-insulin autoantibodies were positive, but no anti–glutamic acid decarboxylase antibodies were detected (Table S4). In 2009, anti-thyroglobulin autoantibodies were detected, but tests for anti-glutaminase, anti-endomysium, and anti-thyroperoxidase antibodies were negative. Celiac disease was therefore excluded. In 2011, the patient was diagnosed with Hashimoto thyroiditis, and tests for anti-thyroperoxidase antibodies were positive (Table S4). The patient was treated with levothyroxine. In 2013, the patient presented with fatigue, nausea, and hepatomegaly. She tested positive for HAV IgM on presentation, consistent with primary HAV infection. Serology and PCR results were negative for HBV (other than the presence of anti-HBs due to prior vaccination), HCV, or HEV. The patient was seropositive for CMV and EBV and negative for HIV and HTLV1 and 2. PCR tests for enterovirus were negative. No liver autoantibodies (anti-NA, anti-SMA, anti-LKM1, anti-LC1, anti-SLA, or anti-mitochondria) were detected, excluding autoimmune hepatitis. The patient had no history of exposure to hepatotoxic drugs, and screening tests for such drugs were negative. Liver function tests were as follows: alanine aminotransferase (ALT), 2,181 IU/liter; aspartate aminotransferase (AST), 2,582 IU/liter; γ-glutamyl transferase (GGT), 73 IU/liter; total bilirubin, 274 µmol/liter; conjugated bilirubin, 173 µmol/liter; prothrombin time (PT), 67%; and Factor V, 100% (Table S5). On day 8 of infection, the patient was hospitalized for incoherent speech, jaundice, appetite loss, gingival bleeding, and petechiae. During physical examination at the emergency unit, the patient was unconscious, with icterus, hepatomegaly, and a fever (40°C). The patient was diagnosed with FVH due to HAV infection. On day 9, liver function tests revealed high levels of cytolysis, with a PT of 14%, factor V levels at 30%, and a Glasgow coma scale score of 8 (Table S5). The patient underwent liver transplantation but died a day later of multiple organ failure (day 11). Histological examinations of the native and explanted liver showed 95% hepatocellular necrosis with polymorphic inflammation. The patient had been vaccinated against BCG, *Haemophilus influenzae* type b, pneumococcus, flu, HBV, and MMR with no adverse effects. She was not tested for immunodeficiency. Her polymorphonuclear cell counts were consistently in the normal range (Table S6).

Both parents were seropositive for HAV (IgM-negative) and had normal transaminase levels at the time of the patient's illness (data not shown). The patient's two siblings (III.2 and III.3) had IgM antibodies against HAV and were admitted to hospital 2 d after she died, but neither developed FVH. The patient's older brother (III.2), born in 2005, had diarrhea and four vomiting episodes 2 d before hospitalization. On arrival at the hospital, his clinical examination was normal, with no fever, weight loss, icterus, encephalopathy, or hepatosplenomegaly. His laboratory findings on day 1 were as follows: ALT, 42 IU/liter; AST, 44 IU/liter; GGT, 55 IU/liter; hemoglobin, 14.8 g/dl; total bilirubin, 6 µmol/liter; C-reactive protein <5; and PT, 100%. Basic metabolic tests gave normal results. The findings on day 2 were as follows: ALT, 35 IU/liter; AST, 36 IU/liter; GGT, 48 IU/liter; total bilirubin, 10 µmol/liter; and PT, 89%. Acute HAV infection was diagnosed. On day 3, no vomiting or diarrhea was observed. Hepatic data had returned to normal except for GGT (41 IU/liter), PT (100%), and Factor V (93%; Table S5).

The patient's other sibling (III.3), born in 2011, had no symptoms before hospitalization. Clinical examination was normal on arrival at the hospital, and laboratory findings were as follows: ALT, 1,594 IU/liter; AST, 755 IU/liter; GGT, 293 IU/liter; total bilirubin, 10 µmol/liter; and PT, 92%. Laboratory findings on day 2 were as follows: ALT, 1,298 IU/liter; AST, 513 IU/liter; GGT, 277 IU/liter; and total bilirubin, 11 µmol/liter. Acute HAV infection was diagnosed. Laboratory findings on day 3 were as follows: ALT, 894 IU/liter; AST, 271 IU/liter; GGT, 229 IU/liter; total bilirubin, 7 µmol/liter; PT, 100%, and Factor V, 100% (Table S5). This sibling suffered one episode of diarrhea and vomiting. By day 4, both siblings were discharged from the hospital. None of the parents or siblings has ever had any other symptoms of hepatitis or another liver disease to date.

WES and genetic analysis

gDNA extraction, WES data collection, and analyses were performed as previously described (Belkaya et al., 2017; Regateiro

et al., 2017). Briefly, allele frequencies (AFs) were obtained from the National Heart, Lung, and Blood Institute Gene Ontology Exome Sequencing Project (EVS, ESP6500SI-V2 release on http://evs.gs.washington.edu/EVS/), 1000 Genomes Project (April 2014 data release on http://grch37.ensembl.org), and GnomAD (February 2017 data release on http://gnomad.broadinstitute.org/). All variant calls with a genotype quality <20, and a depth of coverage <5 were filtered out. Only indel-inframe, indel-frameshift, start-lost, missense, nonsense, stop-lost, and essential splice-site (splice acceptor and splice donor) variants were retained for further analysis. Given the rare occurrence of FVH in children, we excluded common polymorphisms with an AF of ≥0.1% in public databases: EVS, 1000 Genomes, and GnomAD, including variants with an AF ≥0.1% in each ethnic subpopulation (African, Ashkenazi Jewish, Finnish, non-Finnish European, South Asian, East Asian, and Latino) in GnomAD. In silico predictions of the impact of variants were evaluated with the following algorithms: GDI (http://pec630.rockefeller.edu:8080/GDI/; Itan et al., 2015), CADD (https://cadd.gs.washington.edu/score; Kircher et al., 2014), and MSC (http://pec630.rockefeller.edu:8080/MSC/; Itan et al., 2016). MSC scores were generated with a 99% confidence interval based on the CADD 1.3 scores of all disease-causing mutations in the Human Gene Mutation Database, regardless of the gene concerned (Itan et al., 2016).

Sanger sequencing of gDNA

We validated genomic variants in patients and their relatives by amplifying 200–300-bp regions encompassing the mutation from gDNA samples with different sets of site-specific primers (Seq-1 and Seq-2 forward/reverse primer sets) listed in Table S7. The amplicons were then sequenced with BigDye Terminator technology on an ABI 3730 DNA sequencer. SnapGene (Version 3.1.4) was used for sequence analysis.

Gene expression analyses

EBV-B cells were generated as previously described (Durandy et al., 1997) and cultured in Roswell Park Memorial Institute (RPMI) 1640 medium supplemented with 10% FBS. Total RNA was isolated with a Qiagen RNeasy kit, using EBV-B cells from healthy controls and the healthy siblings and parents of the patient. For qPCR analysis, cDNA samples generated with oligo-dT primer and the SuperScript III First-Strand Synthesis System (Thermo Fisher Scientific) were used to determine the relative levels of *IL18BP* expression, by amplification of the cDNA generated with TaqMan Universal PCR Master Mix and various TaqMan probes detecting the transcript variants encoding IL-18BPa: Hs00931914 (probe 1), Hs00931907 (probe 2), Hs00931908 (probe 3), and Hs00934414 (probe 4; Thermo Fisher Scientific). We used an Applied Biosystems 7500 Fast Real-Time PCR system with the following program: 50°C for 2 min, 95°C for 10 min, 40 cycles of 95°C for 15 s, and 60°C for 1 min. We calculated qPCR efficiency and the amplification factor for each assay by the standard curve method (Nolan et al., 2006) and used them to determine relative expression levels for *IL18BP* normalized against endogenous *GAPDH* (4310884E; Thermo Fisher Scientific) expression in each sample. For relative quantification of the WT and mutant *IL18BP* transcript variants, we used PowerUp SYBR Green Master Mix (Thermo Fisher Scientific) on an Applied Biosystems 7500 Fast Real-Time PCR system with the following program: 50°C for 2 min, 95°C for 2 min, 35 cycles of 95°C for 15 s, 63°C for 1 min, and 72°C for 30 s (data collection), followed by the melting curve protocol: 95°C for 15 s, 63°C for 1 min, 95°C for 30 s (1% ramp-rate), and 60°C for 15 s. The primer pairs for each mutant variant (M1, M2, and M3) were designed with the NCBI Primer-BLAST tool (https://www.ncbi.nlm.nih.gov/tools/primer-blast/). The specificity of these primers was assessed by melting curve analysis and confirmed by Sanger sequencing of the qPCR products. Relative copy numbers were determined by the standard curve method with plasmids containing the WT or mutant *IL18BP* sequences, followed by normalization against endogenous *GAPDH* (PrimerBank ID: 378404907c1) levels. The sequences of the SYBR Green qPCR primers are provided in Table S7. All qPCR experiments were performed in duplicate with two independent RNA preparations.

Human hepatoma cells (Hep3B), SV40-transformed human fibroblasts (SV40 fibroblasts) and human hepatic stellate cells (LX-2; Millipore) were cultured in DMEM supplemented with 10% FCS. HUVEC) were cultured in endothelial cell growth medium (Sigma-Aldrich). THP1 (monocytes), Jurkat (T cells), Raji (B cells), and NKL (NK cells) cells were cultured in RPMI-1640 supplemented with 10% FCS. Sodium pyruvate (1 mM) was included in the growth medium for THP1 and NKL cells. NKL cells were cultured in the presence of recombinant human IL-2 (10 ng/ml; Invitrogen). All cell lines (Hep3B cells at 10^6 cells/well, HUVECs at 5×10^5 cells/well, Jurkat cells at 2×10^6 cells/well, LX-2 cells at 10^6 cells/well, NKL cells at 2×10^6 cells/well, Raji cells at 2×10^6 cells/well, SV40 fibroblasts at 5×10^5 cells/well, and THP1 cells at 10^6 cells/well) were plated in fresh medium in 12-well plates on the day before stimulation with various cytokines: IFN-α, 5,000 U/ml (IntronA, IFN-α2b; Schering-Plough); IFN-γ, 1,000 IU/ml (Imukin, IFN-γ1b; Boehringer); TNF-α, 10 ng/ml (R&D Systems); IL-6, 25 ng/ml (R&D Systems); and IL-15, IL-18, IL-22, and IL-29/IFN-λ1, all at 100 ng/ml (R&D Systems). For qPCR analysis, cells were stimulated for 6 h. Total RNA was extracted with the RNeasy Extraction Kit (Qiagen). RNA was reverse-transcribed in High-Capacity RNA-to-cDNA Master Mix (Applied Biosystems). We then performed qPCR in TaqMan assays specific for *IL18* (Hs01038788), *IL18BP* (Hs00931914), *IL18R1* (Hs00977691), and *IL18RAP* (Hs00977695). *GAPDH* (Hs99999905) was used as an endogenous control for *IL18BP*, *IL18R1*, and *IL18RAP*, whereas *HPRT1* (Hs99999909) was used for *IL18*. Relative expression analyses were performed by the dCt method, according to the kit manufacturer's instructions.

Expression of alternative splice forms of *IL18BP* was assessed by PCR amplification with different primer sets ($F_{Ex1\text{-}2}$ and $R_{IL18BPa}$; $F_{Ex1\text{-}2}$ and $R_{IL18BPbd}$; $F_{Ex1\text{-}2}$ and $R_{IL18BPc}$; $F_{Ex2\text{-}3}$ and $R_{IL18BPa}$; $F_{Ex2\text{-}3}$ and $R_{IL18BPbd}$; and $F_{Ex2\text{-}3}$ and $R_{IL18BPc}$) on cDNAs generated using total RNA from HepG2 cells, THP1 cells, and primary human hepatocytes isolated from human liver chimeric mice (unpublished data). The primer sequences are provided in Table S7. For IL-18 and IL-18BP ELISA (DuoSet; R&D Systems), cells

were stimulated for 24 h with the concentrations indicated above. Supernatants were obtained and kept at −80°C. ELISA was performed in accordance with the kit manufacturers' instructions.

Flow cytometry

Unstimulated and stimulated cells were washed with PBS including 2% FCS and 2 mM EDTA. Adherent cell lines were detached with trypsin (Invitrogen) before washing with PBS. Only certain cell lines, HUVECs, LX-2, NKL, and THP1, which had induced *IL18R1* mRNA expression upon stimulation with various cytokines, were stimulated for 24 h, as described above in Gene expression analyses, and further analyzed for surface IL-18R1 expression by flow cytometry. Cells were then fixed with Fix Buffer I (BD biosciences) for 10 min at 37°C and washed twice. Staining was performed using a primary antibody against IL-18R1 (R&D Systems) for 1 h at room temperature, followed by washing and secondary staining with goat IgG (H+L) APC-conjugated Antibody (R&D Systems) for 30 min at room temperature. Cells were washed twice and acquired on a Gallios flow cytometer (Beckman Coulter). Analyses were performed with FlowJo software (FlowJo). Of note, surface IL-18RAP expression on the cell lines above was not assessed, as we did not validate any antibody specific for human IL-18RAP detection by flow cytometry using control transfected cell lines (data not shown).

Rapid amplification of 3′ cDNA ends (3′ RACE) and exon trapping

3′ RACE was performed as previously described (Scotto-Lavino et al., 2006). Briefly, cDNA was synthesized with an adapter primer (AP-1) and SuperScript II Reverse transcription (Thermo Fisher Scientific) from total RNA isolated from the EBV-B cells of a healthy control and the patients' siblings. The first PCR amplification of 3′ partial cDNA ends was performed with a forward primer (F_{Ex1}) specific to *IL18BP* exon 1 and a universal amplification primer (UAP)-1 binding to AP-1. The PCR products were purified and used for nested PCR with an *IL18BP*-specific primer ($F_{Ex1\text{-}2}$) spanning the junction of exons 1 and 2 and an abridged UAP. The final amplicons generated from the WT and heterozygous sibling samples were ligated into the pGEM-T-Easy vector (Promega), and the colonies were sequenced. For in vitro 3′ terminal exon-trapping experiments, 1,558-bp DNA fragments starting with a 3′-fragment of *IL18BP* intron 3 (43 bp) were amplified from the gDNA samples of the WT sibling and the patient, with pTAG4-IL18BP forward and reverse primers. These fragments were between the EcoRI and XhoI sites of the pTAG4 vector. The pTAG4 exon-trapping vector (Krizman and Berget, 1993) was kindly provided by Dr. Anders Lade Nielsen (Aarhus University, Aarhus, Denmark). COS7 cells were transfected with one WT and one mutant clone in the presence of X-tremeGENE 9 DNA Transfection Reagent (Roche). After 16 h, total RNA was extracted with the RNeasy Mini Kit (Qiagen), treated with DNase (Turbo DNA-free Kit; Invitrogen), and used for cDNA synthesis with the SuperScript III First-Strand Synthesis System (Life Technologies) and an adapter primer (AP-2; Blechingberg et al., 2007). The first PCR was performed with a specific primer ($F_{AD1\text{-}2}$) spanning the junction of *AD* exons 1 and 2, and the UAP-2, which binds to AP-2 (Blechingberg et al., 2007). This reaction was followed by nested PCR with a specific primer ($F_{AD2\text{-}Ex4}$) encompassing the junction of *AD* exon 2 and *IL18BP* exon 4 and a reverse primer (R_{UTR}) binding to the end of the *IL18BP* 3′ UTR. The nested PCR products were inserted into the pGEM-T-Easy vector, and the colonies were sequenced. Successful and equivalent cDNA synthesis was confirmed by the amplification by PCR of *HPRT1*, as the housekeeping gene control. SnapGene was used to analyze the DNA sequences of the clones. All clones carrying PCR artifacts or sequences not matching the *IL18BP* canonical transcript were excluded from subsequent analyses. Digital images were captured by the Amersham Imager 600 (GE Healthcare, Life Sciences). The primer sequences are provided in Table S7.

Generation of *IL18BP* constructs and site-directed mutagenesis (SDM)

The human canonical *IL18BP* cDNA open reading frame clone (CCDS8206) was obtained from OriGene and inserted into the pEF-BOS-EX mammalian expression plasmid (Murai et al., 1998), which was kindly provided by Dr. Shigekazu Nagata (Immunology Frontier Research Center, Osaka University, Osaka, Japan). The forward primer (IL18BP BamHI) included a BamHI site and a Kozak consensus sequence, whereas the reverse primer (IL18BP-His XbaI) contained an in-frame coding sequence for a C-terminal 6x-His tag and an XbaI site. SDM to generate the *IL18BP* variants present in GnomAD (p.V23I, p.R121Q, and p.P184L) was performed by a modified overlap-extension PCR-based method (Shimada, 1996). IL18BP BamHI/SDM-reverse primers and SDM-forward/IL18BP-His XbaI primers were used to amplify the mutated *IL18BP* in two separate reactions, using the pEF-BOS-EX-IL18BP-His WT plasmid as the template. Each PCR product was were purified, and the different products were mixed without primers for overlap-extension PCR. SDM for the p.Q192H allele was performed by one-step PCR with the IL18BP BamHI and Q192H-His-XbaI primers. Novel IL18BP transcript variants (M1, M2, and M3) were generated with the IL18BP BamHI and SDM-reverse primers or the SDM-forward and mutant reverse primers (containing an in-frame coding sequence for a C-terminal 6x-His tag, a stop codon, and an XbaI site) in two separate reactions, using the pEF-BOS-EX-IL18BP-His WT plasmid and control gDNA, respectively, as templates. The M1 and M2 transcripts were cloned including an 18-nt polyadenylation insert upstream of the 6x-His tag, followed by a stop codon. All constructs were confirmed by DNA sequencing. The primer sequences are provided in Table S7.

Transient expression of IL-18BP and immunoblotting

COS7 cells were used to seed 6-well plates at a density of 2×10^5 cells/well, in DMEM supplemented with 10% FBS. They were transfected with pEF-BOS-EX-IL18BP-His constructs (500 ng per well) in the presence of the X-tremeGENE 9 DNA transfection reagent (Roche Applied Sciences). The culture medium was removed 6 h after transfection, and the cells were incubated for 3 d in serum-free OptiMEM. Culture supernatants were concentrated by centrifugation on Amicon centrifugal protein

filters (3 kD; EMD Millipore) according to the manufacturer's instructions and stored at −80°C for later use. Total protein concentration in the COS7 supernatants was determined with a Pierce BCA protein assay kit (Thermo Fisher Scientific), and total protein (15 µg protein per lane) was then subjected to SDS/PAGE (12% polyacrylamide gel) under reducing conditions. Immunoblotting was performed with primary antibodies against the His-Tag (MA1-21315, 0.5 µg/ml; Thermo Fisher Scientific) and IL-18BP (AF119, 0.5 µg/ml; R&D Systems). Digital images were captured by the Amersham Imager 600 (GE Healthcare, Life Sciences).

IL-18BP bioassay

The bioactivity of human IL-18BP was assessed by measuring inhibition of the IFN-γ–inducing activity of human IL-18 in NK-92 cells (Kim et al., 2000). Briefly, NK-92 cells were cultured in RPMI supplemented with 10% FBS and 200 IU/ml IL-2 (Chiron). Before the IL-18BP bioassay, NK-92 cells were rested for 24 h in the absence of IL-2. Rested NK-92 cells, at a density of 0.5 × 10^6 cells/ml in flat-bottomed 96-well plates, were stimulated for 24 h with 100 pg/ml IL-12 (R&D Systems), 10 ng/ml IL-18 (R&D Systems), and various concentrations of recombinant IL-18BP-His (125, 250, or 500 ng/ml; Sino Biologicals) or with concentrated supernatants (100 µg/ml of total protein) from COS7 cells transiently transfected with IL-18BP constructs. IL-18 and IL-18BP were mixed together and incubated for 1 h at 37°C before their addition to cells. At 24 h, the supernatants were used for ELISA, to assess IFN-γ production (Human IFN gamma Ready-Set-Go; Thermo Fisher Scientific). All IL-18BP bioassays were performed in duplicate.

Immunohistochemistry

Immunohistochemical staining was performed on 4-µm-thick sections of formalin-fixed paraffin-embedded tissue samples, with Bond autostainer (Leica), after antigen retrieval and endogenous peroxidase inhibition with H_2O_2 (3%). We used primary antibodies against CD3 (polyclonal rabbit, CD3ε, A0452; Dako, Agilent), CD4 (monoclonal IgG1k mouse, NCL-L-CD4-368; Leica), CD8 (monoclonal IgG1k mouse, C8/144B; Dako), CD20 (monoclonal IgG2ak mouse, L26; Dako), CD57 (monoclonal IgM mouse, NK-1; Leica), CD68 (monoclonal IgG2a mouse, 514H12; Leica), CD163 (monoclonal IgG1 mouse, NCL-L-CD163; Leica), perforin (monoclonal IgG1 mouse, 5B10; Leica), NKp46 (polyclonal IgG goat, AF1850; R&D Systems), and Hep Par-1 (monoclonal IgG1k mouse, OCH1E5; Dako). These antibodies were detected, and the signal was amplified with the Bond Polymer Refine Detection kit (DS9800; Leica) and hematoxylin counterstaining. We also used primary antibodies against IL-18BP (monoclonal mouse, clone 13603; R&D Systems), IL-18BP (polyclonal rabbit, HP37434; Sigma-Aldrich), and IL-18 (polyclonal rabbit, HPA0003980; Sigma-Aldrich). These antibodies were detected, and the signal was amplified with the Bond Intense R kit (DS9263; Leica) and hematoxylin counterstaining. Native explanted livers are usually fixed in formalin at room temperature for 3–8 d, while most other tissue samples are fixed for 6–72 h. This long immersion in formalin may be responsible for alteration of some epitopes and for increased background signals when performing immunohistochemistry. Moreover, the most efficient kits available for immunohistochemistry include a streptavidin-biotin amplification step. This may also explain the increased background signals during immunohistochemistry staining, as hepatocytes contain endogenous biotin. Although IL-18BP staining was validated on control transfected cell lines, the staining observed in healthy or diseased livers was not significantly different from the staining detected with the diluent without the primary antibody as negative control (unpublished data). Normal liver corresponds to liver parenchyma of a patient who did not receive chemotherapy and underwent surgery for metastasis of colon carcinoma. The sampling was ≥2 cm away from the nearest metastasis.

Coculture experiments and HAV infection

HepG2 cells (kindly provided by Dr. Yosef Shaul, Weizmann Institute of Science, Rehovot, Israel) were used to seed collagen-coated 96-well plates at 1.5 × 10^4 cells/well in DMEM supplemented with 10% FBS and 0.1 mM nonessential amino acids. NK92 cells (1–2 × 10^6 cells/ml in 24-well plates) were stimulated with IL-18 (200 ng/ml) and/or IL-18BP (1,000 ng/ml) in the absence of IL-2 for 18 h. IL-18 and IL-18BP were mixed together and incubated for 1 h at 37°C before their addition to cells. On the day of coculture, HepG2 cells, at 80–90% confluence, were washed once with serum-free RPMI and stained with calcein-AM (0.5 µM; Trevigen) for 30 min at 37°C (Somanchi et al., 2015; Bugide et al., 2018). Calcein-labeled HepG2 cells were washed twice with complete RPMI. Activated NK cells, washed and resuspended in complete RPMI, were added at a density of 1–3 × 10^5 cells/well to HepG2 cells, and the two cell types were cocultured at 37°C for 4 h. PBMCs from healthy donors were isolated by Ficoll-Paque density gradient, as previously described (Hernandez et al., 2018). Isolated PBMCs (4 × 10^6 cells/ml in 24-well plates) were stimulated with IL-18 (200 ng/ml) and/or IL-18BP (1,000 ng/ml) in the presence of IL-2 (400 IU/ml) for 24 h. Stimulated PBMCs, washed and resuspended in complete RPMI, were cultured at various densities (2–4 × 10^5 cells/well) with HepG2 cells for 4 h.

HepG2 and Huh7.5 cells were infected with HAV (HM-175/18f) at various dilutions and maintained in DMEM supplemented with 3% FBS and 0.1 mM nonessential amino acids for several days. 3 d after infection, when HepG2 and Huh7.5 cells reached maximum infection rates of ~40 and ~100%, respectively, both mock- and HAV-infected hepatocytes were detached and reseeded on collagen-coated 96-well plates at 1.5 × 10^4 cells/well. Surplus infected cells were lysed for RNA isolation, and their supernatants were stored for future use. On the following day, calcein-labeled mock- or HAV-infected HepG2 cells were cultured with NK-92 cells (3 × 10^5 cells/well), which were activated with IL-18 and/or IL-18BP, as described above. For Huh7.5 cells, NK-92 cells were stimulated with IL-18 (200 ng/ml) and/or IL-18BP (1,000 ng/ml) in the presence of IL-2 (20 IU/ml) for 18 h and cultured at 3 × 10^5 cells/well with calcein-labeled mock- or HAV-infected Huh7.5 cells. After 4 h of coculture, supernatants were collected and stored at −80°C for later use. Cells were washed twice with PBS and fixed by incubation with 4% PFA for 20 min at room temperature in the dark. The nuclei were then

stained with DAPI (D1306 at 1:5,000; Thermo Fisher Scientific). For high-content imaging analyses, ImageXpress Micro XLS (Molecular Devices) and MetaXpress PowerCore software were used. The total-cell integrated intensity of calcein-positive cells was determined for each well and adjusted by subtracting the background fluorescence (unstained hepatocyte cells). As an alternative to fluorescence imaging, albumin levels in hepatocyte–NK cell cocultures were determined by ELISA, as previously described (de Jong et al., 2014). Relative fluorescence and albumin levels were determined by normalization against the mean value for hepatocytes cocultured with effector cells (NK-92 cells or PBMCs) without pretreatment, set to 100. All coculture experiments were performed in quadruplicate.

For HAV immunostaining, infected hepatocytes were fixed with 4% PFA for 30 min at room temperature. Fixed cells were washed twice with PBS and incubated with 100 mM glycine for 15 min. Cells were then permeabilized for 10 min using PBS with 0.1% Triton X-100, followed by blocking for 1 h with PBS + 5% goat serum (005-000-121; Jackson ImmunoResearch). Cells were stained with primary antibodies against HAV (mouse anti-HAV VP1, K2-4F2; Creative Biolabs; mouse anti-HAV, 7E7; Mediagnost) at 1:1,000 overnight at 4°C, followed by staining with goat anti-mouse Alexa Fluor 594 at 1:1,000 and DAPI at 1:5,000 for 1 h at room temperature. All antibody dilutions were performed in PBS + 5% goat serum. Finally, cells were imaged using a Nikon Eclipse TE300 fluorescent microscope, and images were processed with ImageJ (National Institutes of Health). Total RNA and supernatants harvested from infected HepG2 and Huh7.5 cells were used for expression analysis of *IL18* and *IL18BP* by qPCR and ELISA, as described above; however no mRNA and protein induction of *IL18* or *IL18BP* was detected in HAV-infected HepG2 or Huh7.5 hepatocytes (data not shown).

Statistical analysis

The results of the experiments were plotted as means ± SEM. GraphPad Prism software was used to calculate mean values and SEM and for one-way ANOVA. Statistical significance is indicated by asterisks (*, $P < 0.05$; **, $P < 0.01$; and ***, $P < 0.001$), with P values >0.05 considered nonsignificant.

Data availability

The WES data are available in the Sequence Read Archive with the BioProject accession no. PRJNA543035.

Online supplemental material

Fig. S1 depicts the impact of *IL18BP*:c.508-19_528del on gene expression and function. Figs. S2 and S3 show the expression patterns of IL-18, IL-18BP, and IL-18R in various human cell lines. Fig. S4 presents the liver immunohistochemistry profile of patients with FVH. Fig. S5 shows IL-18/IL-18BP–mediated hepatotoxicity. Table S1 summarizes the genetic analysis of the WES data of the patient and two siblings. Table S2 lists the homozygous rare nonsynonymous variations present only in the patient. Table S3 describes the characteristics of genes with homozygous rare nonsynonymous variations present only in the patient. Table S4 provides other clinical findings of the patient before FVH. Table S5 shows the analytical findings in the patient and her siblings during the course of HAV infection. Table S6 presents the immunological phenotyping data of the patient during the course of HAV infection. Table S7 lists the primers used in this study.

Acknowledgments

We thank the patient and family for participating in this study. We thank the members of the pediatric medical staff of Bicêtre Hospital, Paris, France, Dr. Dalila Habes, Dr. Charlotte Mussini, Dr. Laurent Chevret, Dr. Philippe Rouleau, and Dr. Hélène Martelli, for taking care of the patients, and Dr. Jean-Louis Salomon (Mantes Hospital, Mantes la Jolie, France) for referring the patient. We also thank Dr. Philippe Gaulard (Groupe Hospitalier Henri Mondor, Créteil, France) for his help with histopathology and Dr. Mohsan Saeed (Laboratory of Virology and Infectious Disease, The Rockefeller University, New York, NY) for his help with HAV infection studies. We thank the Genomics Resource Center and the High-Throughput Screening Resource Center at the Rockefeller University and several members of the St. Giles Laboratory of Human Genetics of Infectious Diseases, Yelena Nemirovskaya, Dominick Papandrea, Mark Woollett, Cécile Patissier, and Tatiana Kochetkov, for administrative and technical assistance; Yuval Itan, Franck Rapaport, Benedetta Bigio, and Matthieu Bouaziz for assistance with bioinformatics; and Rui Yang and Shen-Ying Zhang for highly pertinent intellectual discussions.

This study was supported under the "Investments for the future" program (Agence Nationale de la Recherche, ANR-10-IAHU-01), and by Institut National de la Santé et de la Recherche Médicale, Université Paris Descartes, the St. Giles Foundation, the Rockefeller University, and the Howard Hughes Medical Institute (to J.-L. Casanova), the French National Agency for Research on AIDS (18265; to E. Jouanguy), the International PhD program of Imagine Institute, Paris, France (to C.B. Korol), and the National Institute of Allergy and Infectious Diseases of the National Institutes of Health (R01-AI091707; to C.M. Rice). S. Belkaya was sponsored by Clinical and Translational Research Fellowship from the American Association for the Study of Liver Diseases Foundation, Specific Defect Research Program from the Jeffrey Modell Foundation, and the Rockefeller University Center for Basic and Translational Research on Disorders of the Digestive System through the generosity of the Leona M. and Harry B. Helmsley Charitable Trust. The funders had no role in the design and conduct of this study, in the collection, analysis, and interpretation of the data, or in the preparation, review, or approval of the manuscript.

The authors declare no competing financial interests.

Author contributions: S. Belkaya, E. Jouanguy, and J.-L. Casanova conceived the study. L. Lorenzo-Diaz, S. Boucherit, M. Sebagh, E. Jacquemin, E. Jouanguy, and J.-L. Casanova recruited the patient. S. Belkaya designed and carried out the experiments, and performed the analyses with contributions from E. Michailidis, C.B. Korol, M. Kabbani, P. Bastard, and Y.S. Lee. J.-F. Emile performed the immunohistochemistry and interpretation of the data. A. Cobat, N. Hernandez, S. Drutman, Y.P. de Jong, E. Vivier, J. Bruneau, V. Béziat, B. Boisson, L. Abel, and C.M. Rice

contributed to study design and data analyses. S. Drutman and E. Jacquemin participated in writing the case report. S. Belkaya, E. Jouanguy, and J.-L. Casanova wrote the manuscript and designed the figures with input from all authors.

Submitted: 12 April 2019
Revised: 14 May 2019
Accepted: 15 May 2019

References

Aizawa, Y., K. Akita, M. Taniai, K. Torigoe, T. Mori, Y. Nishida, S. Ushio, Y. Nukada, T. Tanimoto, H. Ikegami, et al. 1999. Cloning and expression of interleukin-18 binding protein. *FEBS Lett.* 445:338–342. https://doi.org/10.1016/S0014-5793(99)00148-9

Ajmera, V., G. Xia, G. Vaughan, J.C. Forbi, L.M. Ganova-Raeva, Y. Khudyakov, C.K. Opio, R. Taylor, R. Restrepo, S. Munoz, et al. Acute Liver Failure Study Group. 2011. What factors determine the severity of hepatitis A-related acute liver failure? *J. Viral Hepat.* 18:e167–e174. https://doi.org/10.1111/j.1365-2893.2010.01410.x

Bachmann, M., J. Pfeilschifter, and H. Mühl. 2018. A Prominent Role of Interleukin-18 in Acetaminophen-Induced Liver Injury Advocates Its Blockage for Therapy of Hepatic Necroinflammation. *Front. Immunol.* 9: 161. https://doi.org/10.3389/fimmu.2018.00161

Belkaya, S., A.R. Kontorovich, M. Byun, S. Mulero-Navarro, F. Bajolle, A. Cobat, R. Josowitz, Y. Itan, R. Quint, L. Lorenzo, et al. 2017. Autosomal Recessive Cardiomyopathy Presenting as Acute Myocarditis. *J. Am. Coll. Cardiol.* 69:1653–1665. https://doi.org/10.1016/j.jacc.2017.01.043

Blechingberg, J., S. Lykke-Andersen, T.H. Jensen, A.L. Jørgensen, and A.L. Nielsen. 2007. Regulatory mechanisms for 3′-end alternative splicing and polyadenylation of the Glial Fibrillary Acidic Protein, GFAP, transcript. *Nucleic Acids Res.* 35:7636–7650. https://doi.org/10.1093/nar/gkm931

Bugide, S., M.R. Green, and N. Wajapeyee. 2018. Inhibition of Enhancer of zeste homolog 2 (EZH2) induces natural killer cell-mediated eradication of hepatocellular carcinoma cells. *Proc. Natl. Acad. Sci. USA.* 115: E3509–E3518. https://doi.org/10.1073/pnas.1802691115

Casanova, J.L. 2015a. Human genetic basis of interindividual variability in the course of infection. *Proc. Natl. Acad. Sci. USA.* 112:E7118–E7127.

Casanova, J.L. 2015b. Severe infectious diseases of childhood as monogenic inborn errors of immunity. *Proc. Natl. Acad. Sci. USA.* 112:E7128–E7137.

Casanova, J.L., and L. Abel. 2018. Human genetics of infectious diseases: Unique insights into immunological redundancy. *Semin. Immunol.* 36: 1–12. https://doi.org/10.1016/j.smim.2017.12.008

Casanova, J.L., M.E. Conley, S.J. Seligman, L. Abel, and L.D. Notarangelo. 2014. Guidelines for genetic studies in single patients: lessons from primary immunodeficiencies. *J. Exp. Med.* 211:2137–2149. https://doi.org/10.1084/jem.20140520

de Jong, S.J., A. Créquer, I. Matos, D. Hum, V. Gunasekharan, L. Lorenzo, F. Jabot-Hanin, E. Imahorn, A.A. Arias, H. Vahidnezhad, et al. 2018. The human CIB1-EVER1-EVER2 complex governs keratinocyte-intrinsic immunity to β-papillomaviruses. *J. Exp. Med.* 215:2289–2310. https://doi.org/10.1084/jem.20170308

de Jong, Y.P., M. Dorner, M.C. Mommersteeg, J.W. Xiao, A.B. Balazs, J.B. Robbins, B.Y. Winer, S. Gerges, K. Vega, R.N. Labitt, et al. 2014. Broadly neutralizing antibodies abrogate established hepatitis C virus infection. *Sci. Transl. Med.* 6:254ra129. https://doi.org/10.1126/scitranslmed.3009512

Durandy, A., C. Hivroz, F. Mazerolles, C. Schiff, F. Bernard, E. Jouanguy, P. Revy, J.P. DiSanto, J.F. Gauchat, J.Y. Bonnefoy, et al. 1997. Abnormal CD40-mediated activation pathway in B lymphocytes from patients with hyper-IgM syndrome and normal CD40 ligand expression. *J. Immunol.* 158:2576–2584.

Durst, R.Y., N. Goldsmidt, J. Namestnick, R. Safadi, and Y. Ilan. 2001. Familial cluster of fulminant hepatitis A infection. *J. Clin. Gastroenterol.* 32: 453–454. https://doi.org/10.1097/00004836-200105000-00023

European Association for the Study of the Liver. 2017. EASL Clinical Practical Guidelines on the management of acute (fulminant) liver failure. *J. Hepatol.* 66:1047–1081. https://doi.org/10.1016/j.jhep.2016.12.003

Faggioni, R., R.C. Cattley, J. Guo, S. Flores, H. Brown, M. Qi, S. Yin, D. Hill, S. Scully, C. Chen, et al. 2001. IL-18-binding protein protects against lipopolysaccharide- induced lethality and prevents the development of Fas/Fas ligand-mediated models of liver disease in mice. *J. Immunol.* 167: 5913–5920. https://doi.org/10.4049/jimmunol.167.10.5913

Fantuzzi, G., N.K. Banda, C. Guthridge, A. Vondracek, S.H. Kim, B. Siegmund, T. Azam, J.A. Sennello, C.A. Dinarello, and W.P. Arend. 2003. Generation and characterization of mice transgenic for human IL-18-binding protein isoform a. *J. Leukoc. Biol.* 74:889–896. https://doi.org/10.1189/jlb.0503230

Finotto, S., J. Siebler, M. Hausding, M. Schipp, S. Wirtz, S. Klein, M. Protschka, A. Doganci, H.A. Lehr, C. Trautwein, et al. 2004. Severe hepatic injury in interleukin 18 (IL-18) transgenic mice: a key role for IL-18 in regulating hepatocyte apoptosis in vivo. *Gut.* 53:392–400. https://doi.org/10.1136/gut.2003.018572

Fujiwara, K., O. Yokosuka, K. Fukai, F. Imazeki, H. Saisho, and M. Omata. 2001. Analysis of full-length hepatitis A virus genome in sera from patients with fulminant and self-limited acute type A hepatitis. *J. Hepatol.* 35:112–119. https://doi.org/10.1016/S0168-8278(01)00074-5

Guidotti, L.G., and F.V. Chisari. 2006. Immunobiology and pathogenesis of viral hepatitis. *Annu. Rev. Pathol.* 1:23–61. https://doi.org/10.1146/annurev.pathol.1.110304.100230

Hernandez, N., I. Melki, H. Jing, T. Habib, S.S.Y. Huang, J. Danielson, T. Kula, S. Drutman, S. Belkaya, V. Rattina, et al. 2018. Life-threatening influenza pneumonitis in a child with inherited IRF9 deficiency. *J. Exp. Med.* 215:2567–2585. https://doi.org/10.1084/jem.20180628

Ishiyama, K., H. Ohdan, M. Ohira, H. Mitsuta, K. Arihiro, and T. Asahara. 2006. Difference in cytotoxicity against hepatocellular carcinoma between liver and periphery natural killer cells in humans. *Hepatology.* 43: 362–372. https://doi.org/10.1002/hep.21035

Israel, L., Y. Wang, K. Bulek, E. Della Mina, Z. Zhang, V. Pedergnana, M. Chrabieh, N.A. Lemmens, V. Sancho-Shimizu, M. Descatoire, et al. 2017. Human Adaptive Immunity Rescues an Inborn Error of Innate Immunity. *Cell.* 168:789–800.e10. https://doi.org/10.1016/j.cell.2017.01.039

Itan, Y., L. Shang, B. Boisson, E. Patin, A. Bolze, M. Moncada-Vélez, E. Scott, M.J. Ciancanelli, F.G. Lafaille, J.G. Markle, et al. 2015. The human gene damage index as a gene-level approach to prioritizing exome variants. *Proc. Natl. Acad. Sci. USA.* 112:13615–13620. https://doi.org/10.1073/pnas.1518646112

Itan, Y., L. Shang, B. Boisson, M.J. Ciancanelli, J.G. Markle, R. Martinez-Barricarte, E. Scott, I. Shah, P.D. Stenson, J. Gleeson, et al. 2016. The mutation significance cutoff: gene-level thresholds for variant predictions. *Nat. Methods.* 13:109–110. https://doi.org/10.1038/nmeth.3739

Kaplanski, G. 2018. Interleukin-18: Biological properties and role in disease pathogenesis. *Immunol. Rev.* 281:138–153. https://doi.org/10.1111/imr.12616

Kim, H.Y., M.B. Eyheramonho, M. Pichavant, C. Gonzalez Cambaceres, P. Matangkasombut, G. Cervio, S. Kuperman, R. Moreiro, K. Konduru, M. Manangeeswaran, et al. 2011. A polymorphism in TIM1 is associated with susceptibility to severe hepatitis A virus infection in humans. *J. Clin. Invest.* 121:1111–1118. https://doi.org/10.1172/JCI44182

Kim, J., D.Y. Chang, H.W. Lee, H. Lee, J.H. Kim, P.S. Sung, K.H. Kim, S.H. Hong, W. Kang, J. Lee, et al. 2018. Innate-like Cytotoxic Function of Bystander-Activated CD8$^+$ T Cells Is Associated with Liver Injury in Acute Hepatitis A. *Immunity.* 48:161–173.e5. https://doi.org/10.1016/j.immuni.2017.11.025

Kim, S.H., M. Eisenstein, L. Reznikov, G. Fantuzzi, D. Novick, M. Rubinstein, and C.A. Dinarello. 2000. Structural requirements of six naturally occurring isoforms of the IL-18 binding protein to inhibit IL-18. *Proc. Natl. Acad. Sci. USA.* 97:1190–1195. https://doi.org/10.1073/pnas.97.3.1190

Kimura, K., S. Sekiguchi, S. Hayashi, Y. Hayashi, T. Hishima, M. Nagaki, and M. Kohara. 2011. Role of interleukin-18 in intrahepatic inflammatory cell recruitment in acute liver injury. *J. Leukoc. Biol.* 89:433–442. https://doi.org/10.1189/jlb.0710412

Kircher, M., D.M. Witten, P. Jain, B.J. O'Roak, G.M. Cooper, and J. Shendure. 2014. A general framework for estimating the relative pathogenicity of human genetic variants. *Nat. Genet.* 46:310–315. https://doi.org/10.1038/ng.2892

Krizman, D.B., and S.M. Berget. 1993. Efficient selection of 3′-terminal exons from vertebrate DNA. *Nucleic Acids Res.* 21:5198–5202. https://doi.org/10.1093/nar/21.22.5198

Lebel-Binay, S., A. Berger, F. Zinzindohoué, P. Cugnenc, N. Thiounn, W.H. Fridman, and F. Pagès. 2000. Interleukin-18: biological properties and clinical implications. *Eur. Cytokine Netw.* 11:15–26.

Le Bouteiller, P., A. Barakonyi, J. Giustiniani, F. Lenfant, A. Marie-Cardine, M. Aguerre-Girr, M. Rabot, I. Hilgert, F. Mami-Chouaib, J. Tabiasco, et al. 2002. Engagement of CD160 receptor by HLA-C is a triggering mechanism used by circulating natural killer (NK) cells to mediate

cytotoxicity. *Proc. Natl. Acad. Sci. USA.* 99:16963–16968. https://doi.org/10.1073/pnas.012681099

Lemon, S.M., J.J. Ott, P. Van Damme, and D. Shouval. 2017. Type A viral hepatitis: A summary and update on the molecular virology, epidemiology, pathogenesis and prevention. *J. Hepatol.* 68:167–184. https://doi.org/10.1016/j.jhep.2017.08.034

Liu, M., C.W. Chan, I. McGilvray, Q. Ning, and G.A. Levy. 2001. Fulminant viral hepatitis: molecular and cellular basis, and clinical implications. *Expert Rev. Mol. Med.* 2001:1–19. https://doi.org/10.1017/S1462399401002812

MacPhee, P.J., V.J. Dindzans, L.S. Fung, and G.A. Levy. 1985. Acute and chronic changes in the microcirculation of the liver in inbred strains of mice following infection with mouse hepatitis virus type 3. *Hepatology.* 5:649–660. https://doi.org/10.1002/hep.1840050422

Martínez-Barricarte, R., J.G. Markle, C.S. Ma, E.K. Deenick, N. Ramírez-Alejo, F. Mele, D. Latorre, S.A. Mahdaviani, C. Aytekin, D. Mansouri, et al. 2018. Human IFN-γ immunity to mycobacteria is governed by both IL-12 and IL-23. *Sci. Immunol.* 3:eaau6759. https://doi.org/10.1126/sciimmunol.aau6759

Murai, K., H. Murakami, and S. Nagata. 1998. Myeloid-specific transcriptional activation by murine myeloid zinc-finger protein 2. *Proc. Natl. Acad. Sci. USA.* 95:3461–3466. https://doi.org/10.1073/pnas.95.7.3461

Nielsen, C.M., A.S. Wolf, M.R. Goodier, and E.M. Riley. 2016. Synergy between Common γ Chain Family Cytokines and IL-18 Potentiates Innate and Adaptive Pathways of NK Cell Activation. *Front. Immunol.* 7:101. https://doi.org/10.3389/fimmu.2016.00101

Nolan, T., R.E. Hands, and S.A. Bustin. 2006. Quantification of mRNA using real-time RT-PCR. *Nat. Protoc.* 1:1559–1582. https://doi.org/10.1038/nprot.2006.236

Novick, D., S.H. Kim, G. Fantuzzi, L.L. Reznikov, C.A. Dinarello, and M. Rubinstein. 1999. Interleukin-18 binding protein: a novel modulator of the Th1 cytokine response. *Immunity.* 10:127–136. https://doi.org/10.1016/S1074-7613(00)80013-8

Okamura, H., K. Nagata, T. Komatsu, T. Tanimoto, Y. Nukata, F. Tanabe, K. Akita, K. Torigoe, T. Okura, S. Fukuda, et al. 1995. A novel costimulatory factor for gamma interferon induction found in the livers of mice causes endotoxic shock. *Infect. Immun.* 63:3966–3972.

Picard, C., H. Bobby Gaspar, W. Al-Herz, A. Bousfiha, J.L. Casanova, T. Chatila, Y.J. Crow, C. Cunningham-Rundles, A. Etzioni, J.L. Franco, et al. 2018. International Union of Immunological Societies: 2017 Primary Immunodeficiency Diseases Committee Report on Inborn Errors of Immunity. *J. Clin. Immunol.* 38:96–128. https://doi.org/10.1007/s10875-017-0464-9

Regateiro, F.S., S. Belkaya, N. Neves, S. Ferreira, P. Silvestre, S. Lemos, M. Venâncio, J.L. Casanova, I. Gonçalves, E. Jouanguy, and L. Diogo. 2017. Recurrent elevated liver transaminases and acute liver failure in two siblings with novel bi-allelic mutations of NBAS. *Eur. J. Med. Genet.* 60:426–432. https://doi.org/10.1016/j.ejmg.2017.05.005

Sasbón, J.S., D. Buamscha, S. Gianivelli, O. Imventarza, D. Devictor, R. Moreiro, C. Cambaceres, G. Salip, M. Ciocca, M. Cuarterolo, et al. 2010. Clinical implications of hepatitis A virus ribonucleic acid detection and genotyping in acute liver failure in children in Argentina. *Pediatr. Crit. Care Med.* 11:385–389.

Scotto-Lavino, E., G. Du, and M.A. Frohman. 2006. 3′ end cDNA amplification using classic RACE. *Nat. Protoc.* 1:2742–2745. https://doi.org/10.1038/nprot.2006.481

Shao, X., Y. Qian, C. Xu, B. Hong, W. Xu, L. Shen, C. Jin, Z. Wu, X. Tong, and H. Yao. 2013. The protective effect of intrasplenic transplantation of Ad-IL-18BP/IL-4 gene-modified fetal hepatocytes on ConA-induced hepatitis in mice. *PLoS One.* 8:e58836. https://doi.org/10.1371/journal.pone.0058836

Shimada, A. 1996. PCR-based site-directed mutagenesis. *Methods Mol. Biol.* 57:157–165.

Shinoda, M., G. Wakabayashi, M. Shimazu, H. Saito, K. Hoshino, M. Tanabe, Y. Morikawa, S. Endo, H. Ishii, and M. Kitajima. 2006. Increased serum and hepatic tissue levels of interleukin-18 in patients with fulminant hepatic failure. *J. Gastroenterol. Hepatol.* 21:1731–1736. https://doi.org/10.1111/j.1440-1746.2006.04376.x

Somanchi, S.S., K.J. McCulley, A. Somanchi, L.L. Chan, and D.A. Lee. 2015. A Novel Method for Assessment of Natural Killer Cell Cytotoxicity Using Image Cytometry. *PLoS One.* 10:e0141074. https://doi.org/10.1371/journal.pone.0141074

Son, Y.I., R.M. Dallal, R.B. Mailliard, S. Egawa, Z.L. Jonak, and M.T. Lotze. 2001. Interleukin-18 (IL-18) synergizes with IL-2 to enhance cytotoxicity, interferon-gamma production, and expansion of natural killer cells. *Cancer Res.* 61:884–888.

Tangye, S.G., U. Palendira, and E.S. Edwards. 2017. Human immunity against EBV-lessons from the clinic. *J. Exp. Med.* 214:269–283. https://doi.org/10.1084/jem.20161846

Tsutsui, H., K. Matsui, H. Okamura, and K. Nakanishi. 2000. Pathophysiological roles of interleukin-18 in inflammatory liver diseases. *Immunol. Rev.* 174:192–209. https://doi.org/10.1034/j.1600-0528.2002.017418.x

Ushio, S., M. Namba, T. Okura, K. Hattori, Y. Nukada, K. Akita, F. Tanabe, K. Konishi, M. Micallef, M. Fujii, et al. 1996. Cloning of the cDNA for human IFN-gamma-inducing factor, expression in Escherichia coli, and studies on the biologic activities of the protein. *J. Immunol.* 156:4274–4279.

Veenstra, K.G., Z.L. Jonak, S. Trulli, and J.A. Gollob. 2002. IL-12 induces monocyte IL-18 binding protein expression via IFN-gamma. *J. Immunol.* 168:2282–2287. https://doi.org/10.4049/jimmunol.168.5.2282

Wege, H., S. Siddell, and V. ter Meulen. 1982. The biology and pathogenesis of coronaviruses. *Curr. Top. Microbiol. Immunol.* 99:165–200.

Yalniz, M., H. Ataseven, S. Celebi, O.K. Poyrazoğlu, N. Sirma, and I.H. Bahçeitoğlu. 2005. Two siblings with fulminant viral hepatitis A: case report. *Acta Med. (Hradec Kralove).* 48:173–175. https://doi.org/10.14712/18059694.2018.48

Yoshida, Y., Y. Okada, A. Suzuki, K. Kakisaka, Y. Miyamoto, A. Miyasaka, Y. Takikawa, T. Nishizawa, and H. Okamoto. 2017. Fatal acute hepatic failure in a family infected with the hepatitis A virus subgenotype IB: A case report. *Medicine (Baltimore).* 96:e7847. https://doi.org/10.1097/MD.0000000000007847

Yumoto, E., T. Higashi, K. Nouso, H. Nakatsukasa, K. Fujiwara, T. Hanafusa, Y. Yumoto, T. Tanimoto, M. Kurimoto, N. Tanaka, and T. Tsuji. 2002. Serum gamma-interferon-inducing factor (IL-18) and IL-10 levels in patients with acute hepatitis and fulminant hepatic failure. *J. Gastroenterol. Hepatol.* 17:285–294. https://doi.org/10.1046/j.1440-1746.2002.02690.x

Zhang, S.Y., N.E. Clark, C.A. Freije, E. Pauwels, A.J. Taggart, S. Okada, H. Mandel, P. Garcia, M.J. Ciancanelli, A. Biran, et al. 2018. Inborn Errors of RNA Lariat Metabolism in Humans with Brainstem Viral Infection. *Cell.* 172:952–965.e18. https://doi.org/10.1016/j.cell.2018.02.019